ECMOR XIV

Mo A11

Monotone Multiscale Finite Volume Method for Flow in Heterogeneous Porous Media

Y. Wang (Stanford University), H. Hajibeygi* (Delft University of Technology) & H.A. Tchelepi (Stanford University)

SUMMARY

The MultiScale Finite-Volume (MSFV) method is known to produce non-monotone solutions. The causes of the non-monotone solutions are identified and connected to the local flux across the boundaries of primal coarse cells induced by the basis functions. We propose a monotone MSFV (m-MSFV) method based on a local stencil-fix that guarantees monotonicity of the coarse-scale operator, and thus the resulting approximate fine-scale solution. Detection of non-physical transmissibility coefficients that lead to non-monotone solutions is achieved using local information only and is performed algebraically. For these `critical' primal coarse-grid interfaces, a monotone local flux approximation, specifically, a Two-Point Flux Approximation (TPFA), is employed. Alternatively, a local linear boundary condition is used for the basis functions to reduce the degree of non-monotonicity. The local nature of the two strategies allows for ensuring monotonicity in local sub-regions, where the non-physical transmissibility occurs. For practical applications, an adaptive approach based on normalized positive off-diagonal coarse-scale transmissibility coefficients is developed. Based on the histogram of these normalized coefficients, one can remove the large peaks by applying the proposed modifications only for a small fraction of the primal coarse grids. Though the m-MSFV approach can guarantee monotonicity of the solutions to any desired level, numerical results illustrate that employing the m-MSFV modifications only for a small fraction of the domain can significantly reduce the non-monotonicity of the conservative MSFV solutions.

1. Introduction

Increasing demand for efficient and accurate simulation of multiphase flow in large-scale heterogeneous porous media has motivated the development and extension of the MultiScale Finite Volume (MSFV) method. MSFV, which was first proposed for heterogeneous elliptic pressure equations by Jenny et al. (2003), can be viewed as a locally conservative extension of the MultiScale Finite Element (MSFE) method by Hou and Wu (1997). Recent developments of the MSFV method allow for compositional effects and complex wells, making it a promising approach for the next-generation of reservoir flow simulators (Jenny et al. (2006); Lee et al. (2008); Zhou et al. (2011); Zhou and Tchelepi (2008); Hajibeygi and Jenny (2009); Hajibeygi and Tchelepi (2014); Hajibeygi et al. (2011); Wolfsteiner et al. (2006); Jenny and Lunati (2009); Lee et al. (2009); Hajibeygi et al. (2012)).

Compared with MSFE, the MSFV method has the advantage of being locally mass conservative. This advantage, however, comes with strong sensitivity to large contrasts in the local permeability and anisotropy in the transmissibility. To improve the quality of the reconstructed fine-scale solution, iterative MSFV (i-MSFV) strategies have been developed (Hajibeygi et al. (2008); Zhou and Tchelepi (2012); Wang et al. (2014)). In the development of the Algebraic Multiscale Solver (AMS) by Wang et al. (2014), the coarse-scale symmetric-positive-definite system of MSFE is used to reduce the error norm to arbitrarily small values, while MSFV is employed only at the final stage to obtain a conservative velocity field. Having a velocity field that is conservative is a critical requirement for solving the nonlinear transport equations accurately and efficiently. Moreover, local mass conservation allows for adaptive computations and the use of relatively loose tolerances as a function of time (Hajibeygi et al. (2012, 2008); Hajibeygi and Jenny (2011)). Thus, in the context of a multiscale linear solver, the final step of using MSFV to ensure local conservation must be performed in a manner that minmizes the degree of nonmonotonicity in the reconstructed fine-scale pressure solution. To improve the quality of the MSFV solutions for slightly heterogeneous and grid-aligned anisotropic coefficients, a Compact-MSFV (C-MSFV) operator was proposed by Hesse et al. (2008). While the C-MSFV was effective for many grid-aligned anisotropic problems, it does not overcome the problem with nonmonotonicity for highly heterogeneous anisotropic fields. For heterogeneous problems, some improvements were observed by changing the Boundary Conditions (BC) for all local problems (Lunati and Jenny (2007)).

In this work, the cause of the non-physical peaks associated with the MSFV operator for highly heterogeneous problems is identified clearly and resolved. The peaks are associated with the discretization stencil of coarse nodes that are surrounded by low-permeability regions. It is shown that for these critical coarse nodes, integration of the flux induced by the dual basis functions can result in negative transmissibilities for the coarse-scale pressure system. A monotone MSFV (m-MSFV) method is devised on the basis of local stencil-fix approach, which guarantees the monotonicity of the MSFV solution. The critical interfaces with non-physical transmissibility values for the coarse-scale system are detected algebraically. Then, a local Two-Point-Flux-Approximation (TPFA) scheme is used to calculate the coarse-scale entries for the critical coarse faces only. In addition, the Linear Boundary Condition (LBC) can be employed for the basis function calculations of the critical regions. The LBC-based m-MSFV reduces the norm of non-physical peaks (reducing nonmonotonicity). In contrast to the TPFA-based approach, however, the LBC-based m-MSFV cannot remove all the negative (non-physical) transmissibilies from the coarse-scale system.

The local nature of m-MSFV allows it to be employed adaptively in space and time. In this paper, a histogram of the critical interfaces is calculated based on a normalized value of the non-physical transmissibility coefficients. Then, based on a threshold value, only critical interfaces with large values are detected and fixed. This threshold-based approach allows for minimizing the trade-off between the accuracy and monotonicity of the solutions.

The paper proceeds as follows. After a short review of the MSFV method, in Section 2, the MSFV

coarse-scale operator (system) is described in detail. In Section 3, the m-MSFV method is presented. Numerical results are shown in Section 4, followed by Section 5 where the paper is concluded.

2. Multiscale Finite Volume Method

The elliptic equation for pressure, p, can be written as

$$-\nabla \cdot (\boldsymbol{\lambda} \cdot \nabla p) = q, \tag{1}$$

where the highly heterogeneous mobility (assumed diagonal) tensor and the source terms are denoted with $\boldsymbol{\lambda}$ and q, respectively. The problem (1) is well-posed for a d-dimensioanl computational domain $\Omega \subset \Re^d$, subject to proper boundary conditions at $\partial\Omega \subset \Re^{d-1}$. The discrete form of (1) at the given fine-scale (denoted here on by superscript f), where the coefficients $\boldsymbol{\lambda}$ are computed using a finite-volume Two-Point-Flux-Approximation (TPFA) scheme (Aziz and Settari (2002)), can be written as

$$A^f p^f = q^f, \tag{2}$$

where entries of the transmissibility matrix A^f are $a^f_{ij}|_{i\neq j} = -\frac{\bar{\boldsymbol{\lambda}}_{ij}\cdot\vec{n}_{ij}}{\delta x_{ij}} \cdot \vec{n}_{ij}\delta A_{ij}$. Here, $\bar{\boldsymbol{\lambda}}_{ij}$, δA_{ij} and δx_{ij} are the harmonically averaged permeability, differential element cross section area and the distance between the computational nodes i and j, respectively. Also, the normal unit vector $\vec{n}_{ij}$ points out of volume i at its cross section with cell j. Note that $a^f_{ij} = a^f_{ji}$ and $a^f_{ii} = -\sum_{j=1,j\neq i}^{N_f} a^f_{ij}$, where N_f is the number of fine-scale finite volumes, also hold. In our implementation, the positive definite mobility tensor leads to non-positive off-diagonal ($a^f_{ij}|_{i\neq j} \leq 0$) and non-negative diagonal ($a^f_{ii} \geq 0$) entries for the transmissibility matrix.

The MSFV method employs primal- ($\breve{\Omega}^c$) and dual- ($\tilde{\Omega}^h$) coarse grids superimposed on the given fine grid (Fig. 1). The fine-scale pressure field is constructed as follows:

$$p^f \approx p^{MS} = \sum_{k=1}^{N_c} \Phi_k \breve{p}_k, \tag{3}$$

where N_c represents the number of coarse-scale control volumes. The locally computed basis functions Φ_k are used to prolong the coarse-scale solution $\breve{p}_k$ onto the fine-scale resolution. Basis functions are first computed on dual-coarse cells, $\tilde{\Omega}^h$, and then assembled for all dual cells, N_d, i.e., $\Phi_k = \sum_{h=1}^{N_d} \Phi^h_k$. Note that the precomputed correction term at the fine-scale, Ψ, can be used to improve this approximation, leading to $p^f \approx p' = p^{MS} + \Psi$. The correction term is an independent stage to improve the multiscale solution, p^{MS}. Note that the correction term does not modify the coarse-scale system matrix; hence, we do not consider it in our analysis. For more detailed analysis of the correction term, we refer to Wang et al. (2014).

The basis functions are local solutions of the governing equation (1), i.e.,

$$-\nabla \cdot (\boldsymbol{\lambda} \cdot \nabla \Phi^h_k) = 0 \quad \text{on} \quad \tilde{\Omega}^h \tag{4}$$

$$\Phi^h_k(\boldsymbol{x}_i) = \delta_{ki} \qquad \forall \boldsymbol{x}_i, \tag{5}$$

where δ_{ki} is the Dirac delta function, i.e., $\delta_{ki}|_{k=i} = 1$ and $\delta_{ki}|_{k\neq i} = 0$. Equation (4) subject to (5) at the corner vertices is solvable if a proper boundary condition is imposed on $\partial\tilde{\Omega}^h$. The reduced-dimensional problem condition can be stated as

$$-\nabla_\perp \cdot (\boldsymbol{\lambda} \cdot \nabla \Phi^h_k)_\perp = 0 \quad \text{at} \quad \partial\tilde{\Omega}^h, \tag{6}$$

which has been widely used in the multiscale literature. The subscript $\perp$ denotes the normal projection (operator or vector) with respect to the boundary. Alternatively, if one ignores the mobility variation along the boundary, i.e., $\boldsymbol{\lambda} = \boldsymbol{I}$ at $\partial\tilde{\Omega}^h$, the formulation reduces to the Linear Boundary Condition (LBC).

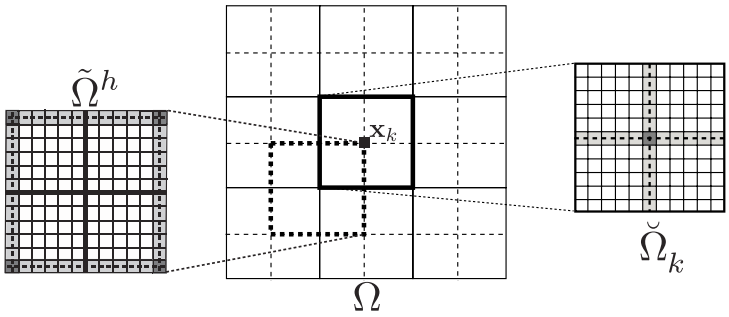

Figure 1 *Illustration of the MSFV primal- and dual-coarse grids imposed on the given 2D computational domain Ω. Zoomed on the right and the left, a primal-coarse $\breve{\Omega}_k$ (coarse control volume) and a dual-coarse $\tilde{\Omega}^h$ (local domain) cells are shown, respectively. A coarse node, $\boldsymbol{x}_k$, here chosen the central cell inside $\breve{\Omega}_k$, is also shown. Boundary cells of local domains (dual-coarse cells) are also highlighted in gray.*

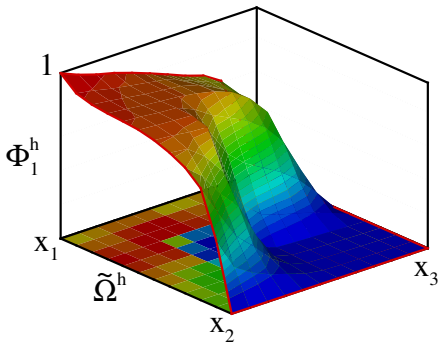

Figure 2 *Illustration of the basis function Φ_1^h solved on dual-coarse cell $\tilde{\Omega}^h$ subject to reduced-dimensional boundary condition. Note that the basis functions are always monotone and satisfy $0 \leq \Phi_k^h \leq 1$, provided that the mobility tensor $\boldsymbol{\lambda}$ is positive definite.*

Note that the basis functions computed with either of the two local boundary conditions are monotone with numerical values between 0 and 1, i.e., $0 \leq \Phi_k(\mathbf{x}) \leq 1 \;\; \forall \mathbf{x} \in \Omega, k = \{1,2,...,N_c\}$, provided that the fine-scale mobility coefficients $\boldsymbol{\lambda}$ are positive definite. Therefore, in the superposition $p^{MS} = \sum \Phi_k \breve{p}_k$, p^{MS} would violate the monotonicity property if and only if the $\breve{p}_k$ violates this property. Hence, all the non-physical peaks are associated with non-physical $\breve{p}_k$ values. This important fact guides us to the cause of the non-physical peaks in the MSFV solution, p^{MS}. That is, the properties of the coarse-scale system control the monotonicity behavior.

The superposition expression is substituted into Eq (1), and integrated over coarse-control volume boundaries. After applying the Gauss integral rule, one obtains the coarse-scale system as

$$A^c \breve{p} = \int_{\breve{\Omega}} q \, d\Omega, \tag{7}$$

where the coarse-scale transmissibility matrix entries a_{ij}^c are

$$a_{ij}^c = -\int_{\partial \breve{\Omega}_i} (\boldsymbol{\lambda} \cdot \nabla \Phi_j) \cdot \vec{n}_i \, d\Gamma. \tag{8}$$

Here, $\vec{n}_i$ is the unit normal vector pointing out of the control volume (coarse-cell) i. Note that $\Phi_j = \sum_{h=1}^{N_d} \Phi_j^h$. Mass conservation leads to

$$a_{ii}^c = -\sum_{j=1, i \neq j}^{N_c} a_{ij}^c = -\int_{\partial \breve{\Omega}_i} (\boldsymbol{\lambda} \cdot \nabla \Phi_i) \cdot \vec{n}_i \, d\Gamma, \tag{9}$$

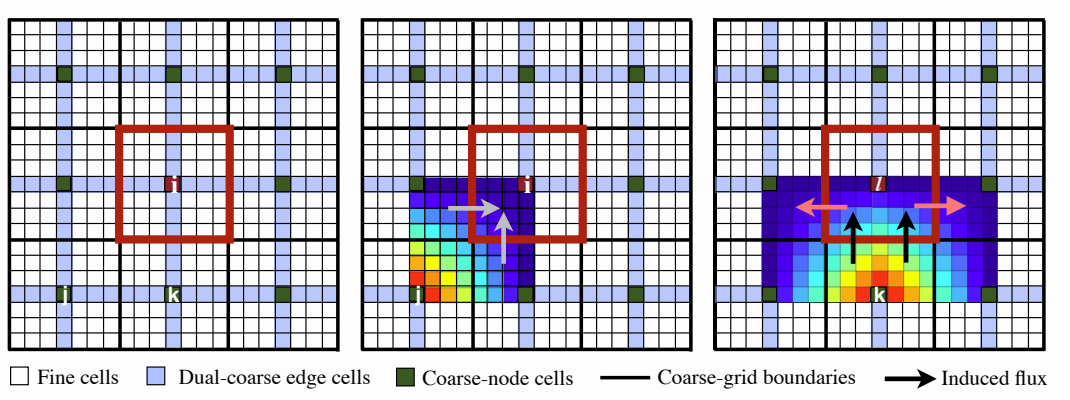

Figure 3 *(left): Illustration of a* 3×3 *coarse- and* 21×21 *fine- grid domain. The coarse cell* i *is highlighted in red, neighboring* k *and* j *on its South and South-West sides. Also shown are the induced fluxes by the* Φ_j *(middle) and* Φ_k *(right). Note that only the overlapping part of the basis functions are plotted, and that for simplicity of the illustration a homogeneous problem is used.*

since $\sum_{j=1}^{N_c} \Phi_j^h = 1$. A coarse-scale system that has positive-definite mobility tensors at the fine scale is expected to yield negative off-diagonal, $a_{ij}^c \leq 0$, and positive diagonal, $a_{ii}^c \geq 0$ values. Note that the coarse-scale system in MSFV is not guaranteed to be symmetric, i.e.,

$$a_{ij}^c = -\int_{\partial \breve{\Omega}_i} (\boldsymbol{\lambda} \cdot \nabla \Phi_j) \cdot \vec{n}_i \, d\Gamma \neq a_{ji}^c = -\int_{\partial \breve{\Omega}_j} (\boldsymbol{\lambda} \cdot \nabla \Phi_i) \cdot \vec{n}_j \, d\Gamma, \tag{10}$$

since the coefficients are integrals of different functions over different control volume boundaries. This is in contrast to the symmetric-positive-definite MSFE coarse-scale operator.

Next, we study the integrals (8) and investigate the situations that may violate this condition.

Coarse-scale Transmissibility Coefficients

In order to study the coarse-scale transmissibility coefficients, a 3×3 coarse-grid problem in 2D is considered in Fig. 3. We study the transmissibility coefficients between cell i and two of its neighboring cells j and k.

For the South-West neighboring cell, i.e., j, the flux induced by the basis function Φ_j, a_{ij}^c, satisfies the physical property of $a_{ij}^c \leq 0$ due to the fact that the both boundary segments of control volume i experience incoming fluxes. Note that the total induced flux (for any heterogeneous field) from j to i needs to be nonnegative.

On the other hand, the fluxes induced by the basis function associated with cell k, Φ_k, must be computed along many (four in 2D) overlapping segments. For cell i, some of these fluxes are incoming and some others are outgoing. For many heterogeneous cases, the net incoming flux to the control volume i is positive, which would lead to a negative off-diagonal entry, which is desirable. Figure 4 shows the SPE 10 bottom layer permeability field which consists of 220×60 fine cells. The MSFV coarse grid is also shown in the figure for a coarsening ratio of 11×5.

Figure 5 shows an extracted rectangular subdomain from Fig. 4, $\tilde{\Omega}^{h1}$, between $(88,5) \leq (x,y) \leq (121,20)$. The location of this extracted domain is highlighted in Fig. 4. Figure 5 also shows that the central coarse cell $(10,3)$ of this subdomain has a net incoming flux induced by the basis function of its southern neighboring cell $(10,2)$, together with the interpolated pressure field only for the associated local domain, i.e., p^{MS} in $\tilde{\Omega}^{h1}$. To obtain this interpolated solution, a test case is solved subject to no-flow Neumann condition on all boundaries and Dirichlet condition of $p = 1$ and $p = 0$ at fine cells $(1,60)$ and

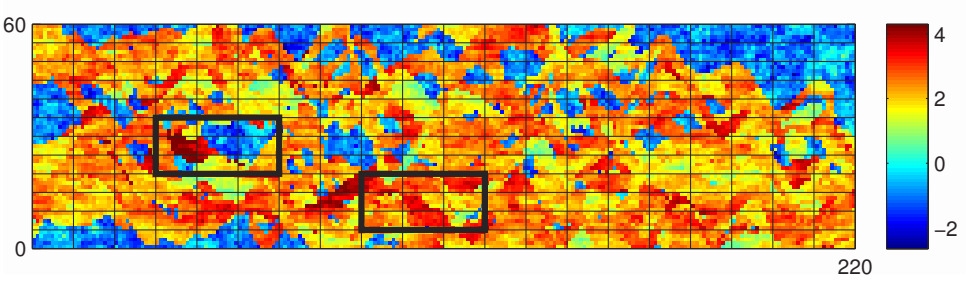

Figure 4 *Logarithm of permeability field for the SPE 10 bottom layer (Christie and Blunt (2001)). The domain consists of* 220×60 *fine- (not shown) and* 20×12 *coarse- (shown) grid cells. Two subdomains of the size* 3×3 *coarse cells are highlighted.*

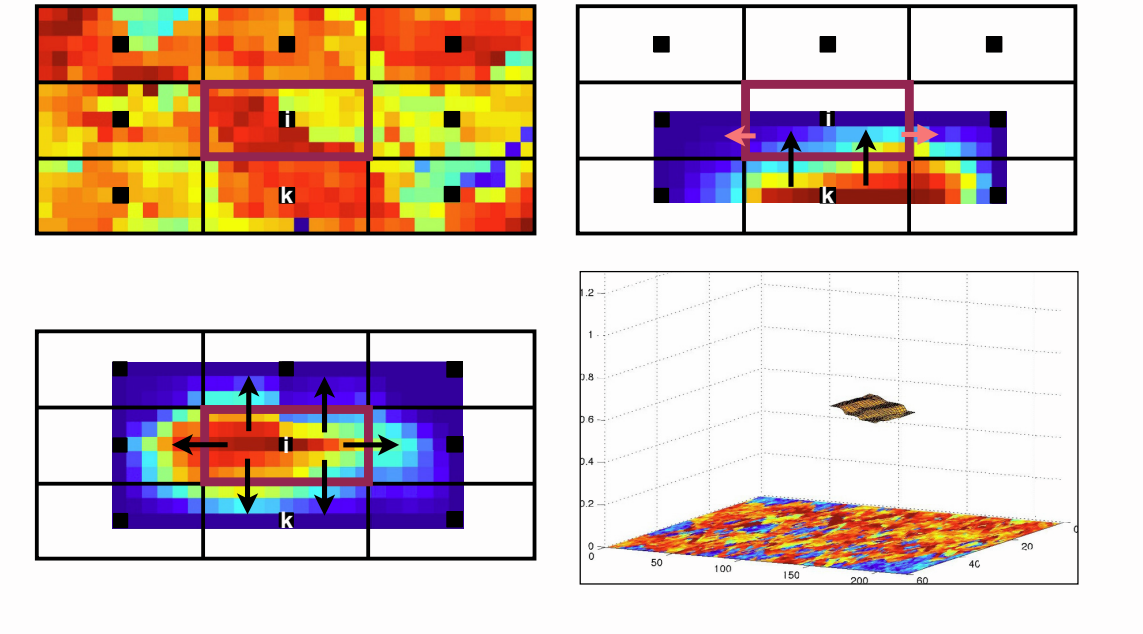

Figure 5 *(top-left): Logarithm of permeability field with coarse grid and coarse nodes, extracted from Fig 4. (top-right): part of the basis function* Φ_k *overlapping with coarse cell i (coarse cell (10,3) in Fig. 4). (bottom-left): basis function* Φ_i*; (bottom-right): superimposed MSFV pressure field,* $p^{MS} = \sum \Phi_k \breve{p}_k$*, obtained for* Ω^{h1}*.*

$(220,1)$, respectively. Note that due to the positive diagonal and negative off-diagonal coarse-system entries corresponding to this local subregion, the interpolated solution is physical.

If for a heterogeneous field, the net incoming flux to the cell i is negative, then positive off-diagonal entries a^c_{ik} are computed. This situation happens when the coarse node $\boldsymbol{x}_i$ lies in a low-permeability region, compared with the other boundary cells between i and k. There are other scenarios that would cause the same situation, e.g., if a shale layer (with very low permeability) crosses the boundary cells between i and k. Note that in such cases, the reduced-problem local boundary condition, between the cells i and k, would lead to a solution with a constant value of one (since the Dirichlet condition at node k is not effective). This constant unity solution, which is then used as a Dirichlet condition for the internal cells, leads to a non-physical outgoing induced flux from the control volume. An example of such a case is illustrated in Fig. 6, where the domain Ω^{h2} is extracted again from (and highlighted in) Fig. 4 for cells belonging to $(33,20) \leq (x,y) \leq (66,35)$ interval. The integral incoming flux induced by Φ_k over the faces of the control volume i is negative, which leads to a positive off-diagonal value of $a^c_{ik} = 222.5$ for the coarse-scale system. The total outgoing fluxes induced by the basis function of i, i.e.,

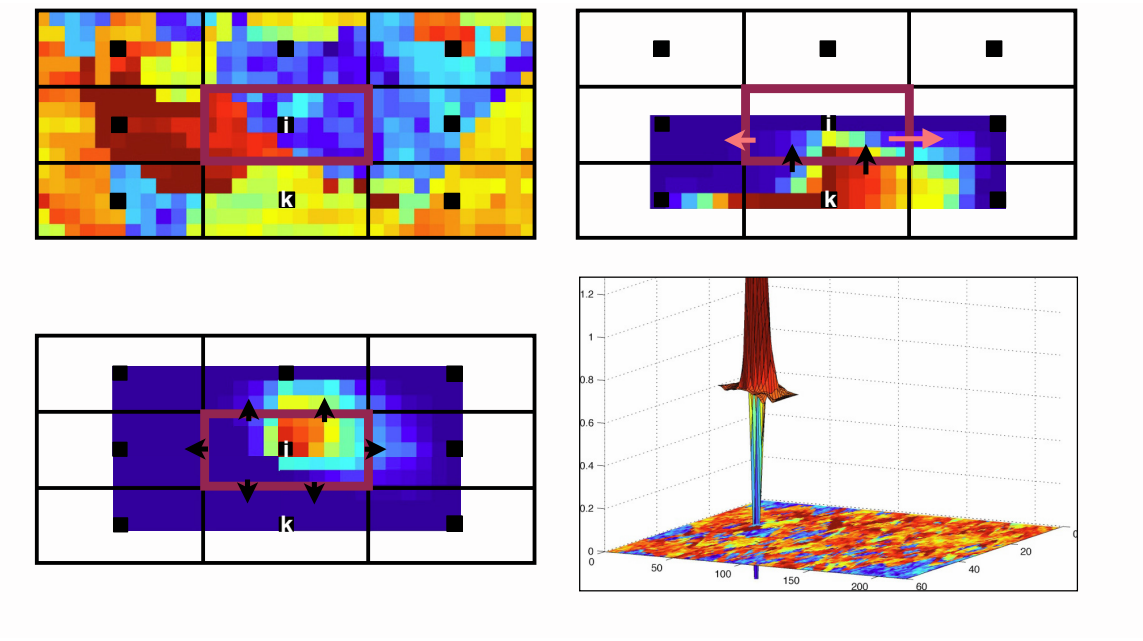

Figure 6 *(top-left): Logarithm of permeability field with coarse grid and coarse nodes, extracted from Fig 4, Ω^{h2}. (top-right): part of the basis function Φ_k overlapping with coarse cell i (coarse cell (5,6) in Fig. 4). (bottom-left): basis function Φ_i; (bottom-right): superimposed MSFV pressure field, $p^{MS} = \sum \Phi_k \check{p}_k$, obtained for Ω^{h2}. Note that a non-physical positive off-diagonal value of $a^c_{ik} = 222.5$ and small positive value of $a^c_{ii} = 0.65$ are calculated for coarse-system entries, which also clearly shows the i-th coarse-system row is not diagonally dominant.*

Φ_i, over its own control volume is too small ($a^c_{ii} = 0.65$), which indicates that the corresponding row in the coarse-scale system is not diagonally dominant. This is closely related to the fact that the coarse node lies in a region with very low permeabilities (blue contour plot in Fig. 6). Note that the other cells (especially the boundary cells) have higher permeability values. As a result, the superimposed MSFV solution entails non-physical peaks (as shown in Fig. 6).

Figure. 7, which is for the SPE 10 bottom layer, indicates that the original MSFV strategy leads to non-physical solutions at several locations. From this figure, it is clear that the peaks are located in regions with high contrasts in the permeability between the neighboring cells. In the next section, we describe a monotone MSFV method.

3. Monotone MSFV (m-MSFV) Method

In this section, to ensure the monotonicity of the MSFV solution, two approaches are proposed. The first one is a local TPFA approach, which automatically detects the interfaces with non-physical transmissibility coefficients for the coarse-scale system. Only for these critical coarse-scale interfaces, a local stencil-fix is employed, where the more stable TPFA stencil is used to calculate the connectivity of the adjacent cells. The second approach is based on employing a Linear Boundary Condition (LBC) to solve the basis functions. Similarly to the local TPFA approach, after detecting the critical coarse-scale interfaces, a LBC is locally applied for the dual-coarse cell boundaries perpenticular to the critical coarse control volume interfaces, while the reduced boundary condition is still used for the other interfaces.

Local TPFA approach

This approach is based on local utilization of a physical flux calculation only for critical faces to ensure monotonicity of the MSFV solution. First, the coarse cell interfaces with negative transmissibility val-

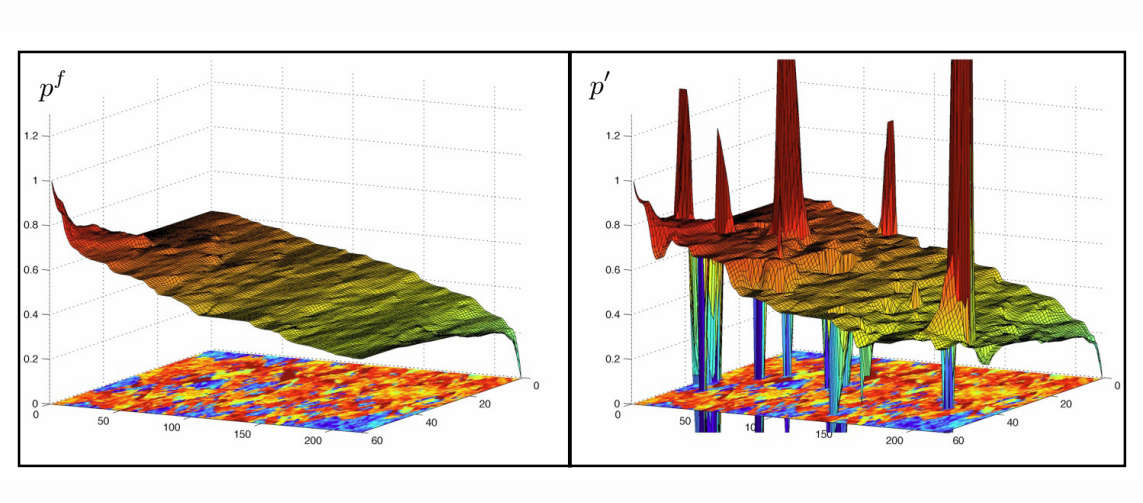

Figure 7 *Fine-scale reference (left) and MSFV (right) solutions for the SPE 10 bottom layer heterogeneous test case. There exist* 220×60 *fine- and* 20×12 *coarse- grid cells. Note that the MSFV superimposed solution entails several non-physical peaks. The permeability field is also partly shown in the plots under the pressure solution.*

ues, i.e., $a^c_{ik} \not\leq 0$, are detected. Then, instead of using the basis functions to provide the a^c_{ik} values with Eq. (8), the transmissibility field between the cell i and k are calculated with TPFA which guarantees that $a^c_{ik} \leq 0$. Figure 8 shows the highlighted pink region used to obtain an effective transmissibility coefficient at the interface between i and k. The procedure to calculate TPFA-based a^c_{ik} is as follows. First, harmonically averaged transmissibility factors among columns of the highlighted pink cells are calculated. Then, the values are summed to compute a^c_{ik}. To ensure conservation, the symmetric entry a^c_{ki} is also updated with the same value as for the a^c_{ik}. Here, the new coarse-scale transmissibilities for the critial faces is computed based on averaging the fine-scale permeability field. Other options such as flow-based upscaling are also possible and can be incorporated into our monotone strategy. In this paper, we focus on our permeability-based strategy. In fact, a slightly positive value a^c_{ij} does not necessarily lead to non-monotone solutions, and only the a^c_{ij} with relatively large positive values matter. Thus, only those critical a^c_{ij} have to be modified. In order to quantify the critical a^c_{ij}, an indicator η_{ij} for each positive off-diagonal entry a^c_{ij} of the coarse-scale coefficients matrix A_c is used. We defined $\eta_{ij} = a^c_{ij}/\omega_i$, where ω_i represents the maximum absolute value of all the negative off-diagonal a^c_{ij} in row i. The coarse node with an interface with $\eta_{ij} > \varepsilon$ is considered critical, where ε is a user-specified threshold value. Then, all the neighbouring interfaces associated with the critical coarse node are replaced by TPFA stencils. Algorithm 1 summarizes how the local TPFA approach is integrated in the MSFV procedure.

Local linear BC approach

In addition to the local TPFA approach, the non-monotonicity of the MSFV pressure solution can be mitigated by locally using a linear BC instead of the reduced BC. For this local linear BC approach, once the critical interface (i.e., the one with $\eta_{ij} > \varepsilon$) is detected, a linear BC is used for the corresponding dual coarse grid boundary perpenticular to the detected interface. For the remaining boundaries, the reduced BC is still used. Then, the basis functions affected by the linear BC are recomputed, and the coarse-scale system is reconstructed. Afterwards, the fine-scale solution is obtained by interplating the coarse-scale solution with the modified basis functions. Finally, the conservative fine-scale velocity field can be constructed by solving local problems with Neumann BC.

The local TPFA approach can guarantees monotonicity of the solution, since the TPFA flux is used over the coarse interfaces. The local linear BC approach can reduce the degree of non-monotonicity;

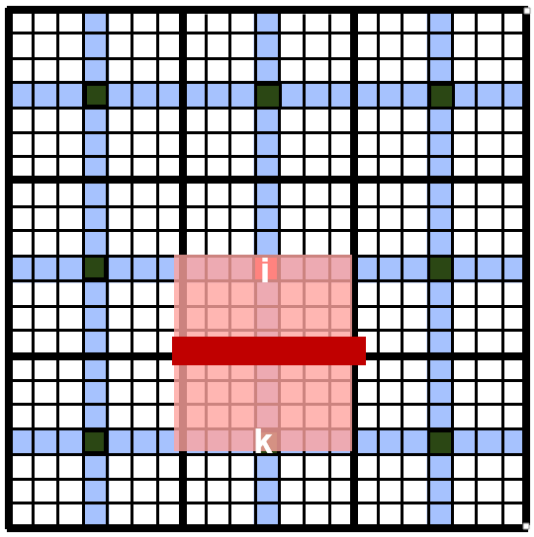

Figure 8 *Automatically detected critical interface (shown in bold red) where* $a_{ik}^{c} \not\leq 0$. *The highlighted region with a pink rectangle shows the local domain, where the transmissibility is calculated using summation of harmonically averaged values to replace with* a_{ik}^{c} *and* a_{ki}^{c}.

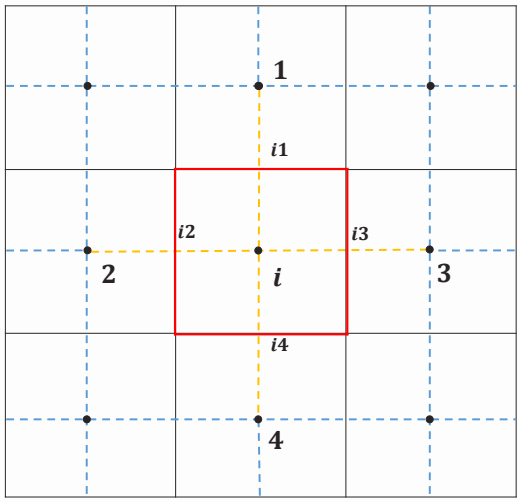

Figure 9 *Critical coarse node* i *and its neighboring faces* F_{ij} *(indicated by red solid lines) and edges* E_{ij} *(indicated by yellow dash lines),* $j = 1,2,3,4$ *for 2D domain. The black lines indicate the coarse volumes.*

Algorithm 1 local TPFA approach integrated with MSFV classical procedure

Construct coarse and dual-coarse grids
Compute basis functions Φ_i and, if needed, correction terms Ψ
Construct coarse-scale system, Eq. (7)
Specify a threshold value ε
for $i = 1$ to N_c **do**
    if $\eta_{ij} > \varepsilon$ **then**
        Cancel the coarse-scale flux through the faces $F_{ij}, j = 1,2,3,4$ as illustrated in Fig. 9
        Calculate TPFA transimissibilities for the faces F_{ij} as T_{ij}^c
        Use TPFA transmissibilities for these faces:
        $a_{ij}^c \leftarrow a_{ij}^c - T_{ij}^c$
        $a_{ii}^c \leftarrow a_{ii}^c + T_{ij}^c$
        $a_{ji}^c \leftarrow a_{ji}^c - T_{ij}^c$
        $a_{jj}^c \leftarrow a_{jj}^c + T_{ij}^c$
    end if
end for
Solve this modified coarse-scale system
Obtain prolongated solution by Eq. (3)
Reconstruct conservative fine-scale velocity field, account for the critical interfaces consistently

however, it cannot guarantee a monotone solution. In addition, the choice of the threshold value, ε, is a trade-off between the computational effort and the degree of monotonicity in the pressure field.

4. Numerical Results

In this section, several test problems are used to illustrate the proposed m-MSFV method. To quantify the accuracy of m-MSFV, relative errors of pressure, velocity and residuals, in terms of L^2 and L^∞ norms, are used. These norms are defined as,

$$\|e_p\| = \|p^m - p^f\| / \|p^o - p^f\|, \tag{11}$$

$$\|e_v\| = \|v^m - v^f\| / \|v^o - v^f\|, \tag{12}$$

$$\|e_r\| = \|r^m - b\| / \|r^o - b\|, \tag{13}$$

where p^m, v^m and r^m denote the pressure, velocity and residual from m-MSFV; p^o, v^o and r^o denote pressure, velocity and residual from original MSFV; p^f, v^f and b represent the fine-scale reference pressure, velocity, and RHS vector (source term). All the pressure plots are scaled by the boundary pressure condition. The local TPFA approach and Linear BC approach are referred to as m-MSFV(TPFA) and m-MSFV(LBC), respectively.

Case 1: SPE 10 bottom layer

The first example is the SPE 10 bottom layer case with 220×60 fine cells and 22×6 coarse cells. The pressure is fixed at (220, 0) and (0, 60) with the values of 1 and 0, respectively; no-flow boundary conditions are specified on all the boundaries. The threshold value $\varepsilon = 0$ indicates the coarse-scale interfaces with positive indicators η_{ij} are all considered as critical interfaces. The permeability and fine-scale reference pressure solution are shown in Fig 10. Since the problem is elliptic, the pressure should be bounded by the pressure values at boundaries (i.e., 0 and 1). However, as shown in Fig 11(a), the original MSFV pressure exceeds these bounds at several locations, which indicates that the obtained solution is nonmonotone. A strictly monotone MSFV pressure can be obtained by using m-MSFV(TPFA), as shown in Fig 11(b). In this case, the m-MSFV(LBC) can also reduce the level of nonmonotonicity significantly as shown in Fig. 11(c); however, this approach cannot guarantee that the solution is monotone.

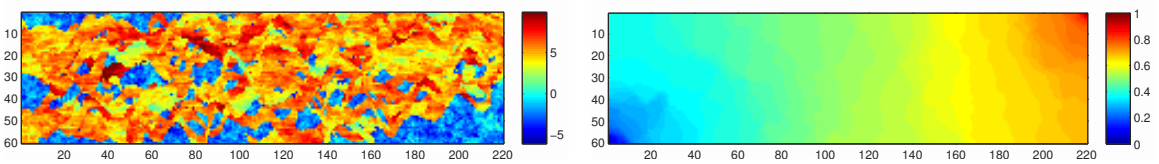

(a) Natural logarithm of the permeability (b) Fine-scale reference pressure

Figure 10 *Natural logarithm of the permeability (a) and fine-scale reference pressure (b) for the SPE 10 bottom layer.*

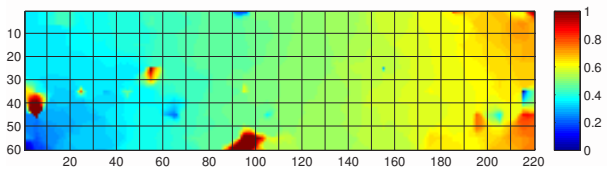

(a) Original MSFV ($\|e_p\|_2 = 0.197$; $\|e_p\|_\infty = 3.815$)

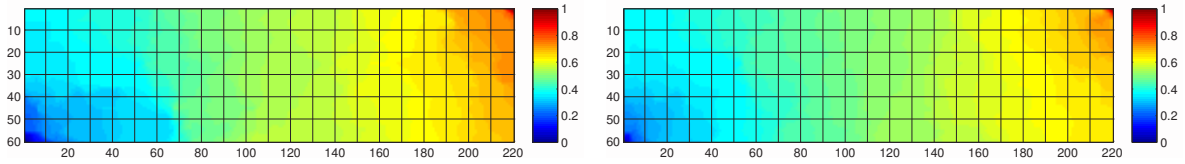

(b) m-MSFV(TPFA) ($\|e_p\|_2 = 0.035$; $\|e_p\|_\infty = 0.071$) (c) m-MSFV(LBC) ($\|e_p\|_2 = 0.052$; $\|e_p\|_\infty = 0.122$)

Figure 11 *Original MSFV and m-MSFV pressure solutions for the SPE 10 bottom layer, and the relative errors e_p. The coarse-scale grids are indicated by black lines.*

Figure 12 shows the streamlines based on the reconstructed velocity fields associated with fine-scale reference pressure obtained using the original and monotone MSFV schemes. As shown in Fig 12(b), the non-physical MSFV pressure leads to circulations in the velocity field, which can decrease the stability of the entire nonlinear simulation procedure. On the contrary, there are no circulations in the velocity field reconstructed by the monotone MSFV pressure. In addition, as seen from the pressure errors, the m-MSFV method can deliver a monotone pressure solution without sacrificing accuracy.

Figure 13 shows the histogram for indicators η_{ij} of the coarse-scale system A_c for the original MSFV and reconstructed coarse-scale system for both m-MSFV approaches. Note that the original coarse-scale system A_c (Fig. 13(a)) has many positive indicators and spans a wide range. These positive values lead to severely non-monotone pressure solution. With the modification of m-MSFV(TPFA), the positive indicators are reduced to a limited range of small values, which is acceptable to obtain a monotone solution. If zero indicators are desired, additional loops of detection and modification can be performed as described in Algorithm 1. On the other hand, with the modification of m-MSFV (LBC), even though this approach can eliminate some positive indicators, many areas with long-range indicator values still remain. These values may result in a non-monotone solution. Note that the remaining indicators cannot be eliminated by additional modification loops. That is the reason why m-MSFV(LBC) can reduce the level of non-monotonicity, but cannot guarantee to fully resolve the issue for all the problems.

For practical purposes, strictly monotone pressure may not be required; therefore the threshold value ε provides a way to balance the degree of monotonicity and the computational cost of the m-MSFV method. Figure 14 shows that m-MSFV (TPFA) with $\varepsilon = 0$ guarantees that the pressure solution is strictly monotone. When the threshold is loosened to $\varepsilon = 0.7$, the pressure solution still does not encounter severe non-monotone regions, while the computational effort is reduced by 50% compared with the $\varepsilon = 0$ case. Figure 15 shows the accuracy of the m-MSFV method with respect to different strategies and indicates that both m-MSFV(TPFA) and m-MSFV(LBC) have comparable error norms for pressure

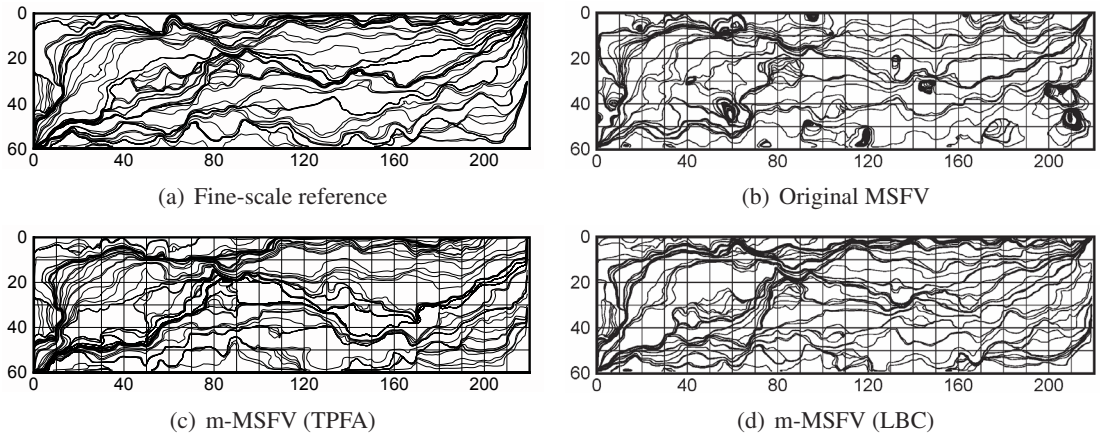

(a) Fine-scale reference (b) Original MSFV

(c) m-MSFV (TPFA) (d) m-MSFV (LBC)

Figure 12 *Streamline plots based on velocity fields reconstructed by fine-scale reference, original and m-MSFV pressure solutions for the SPE 10 bottom layer. The coarse-scale grids are indicated by black lines.*

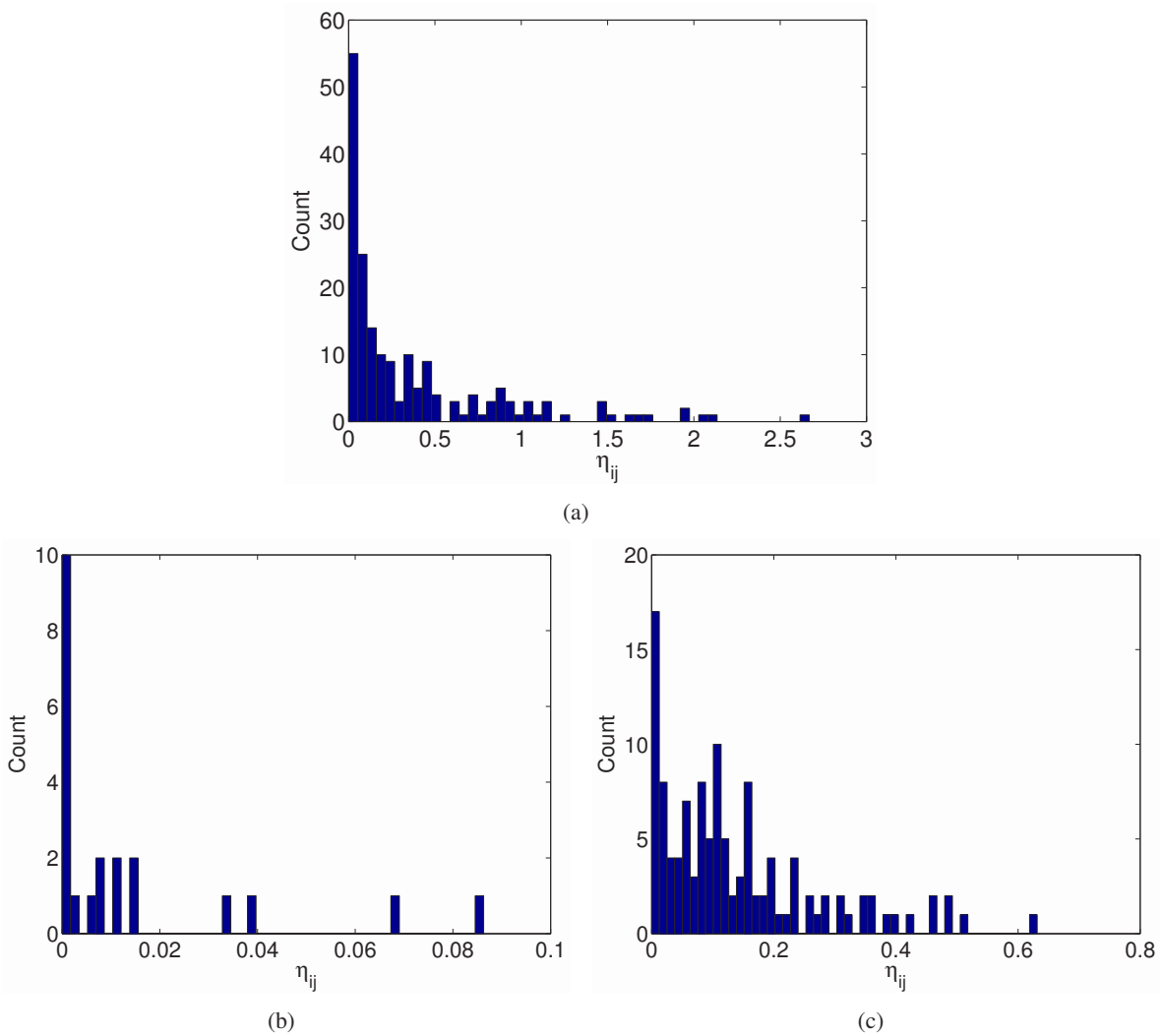

(a)

(b) (c)

Figure 13 *Histogram of η_i of the coarse-scale system A_c for original MSFV (a), the reconstructed coarse-scale system for m-MSFV (TPFA) (b) and m-MSFV (LBC) (c), respectively.*

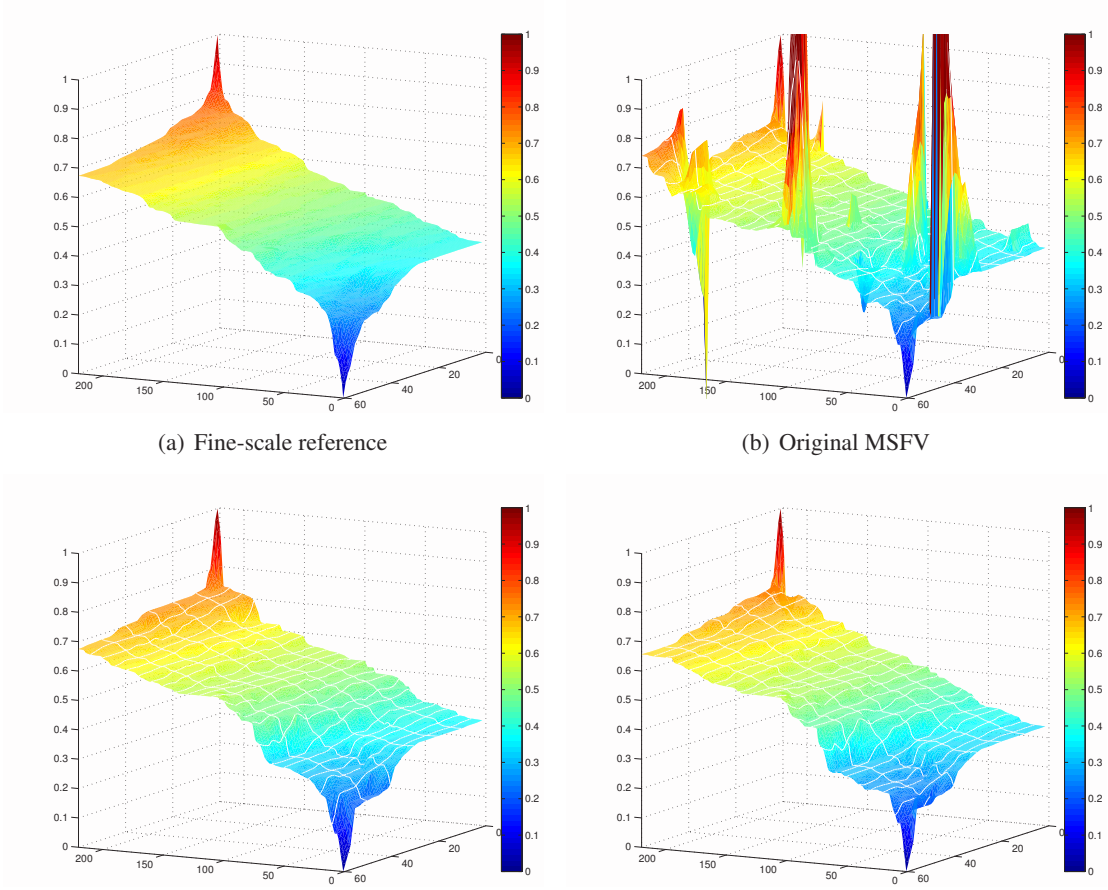

(a) Fine-scale reference

(b) Original MSFV

(c) m-MSFV (TPFA) with $\varepsilon = 0$

(d) m-MSFV (TPFA) with $\varepsilon = 0.7$

Figure 14 *Pressure surface plots for fine-scale reference (a), original MSFV (b), m-MSFV (TPFA) with* $\varepsilon = 0$ *(c) and* $\varepsilon = 0.7$ *(d), respectively*

and velocity. The m-MSFV(LBC) approach results in slightly better residual estimates.

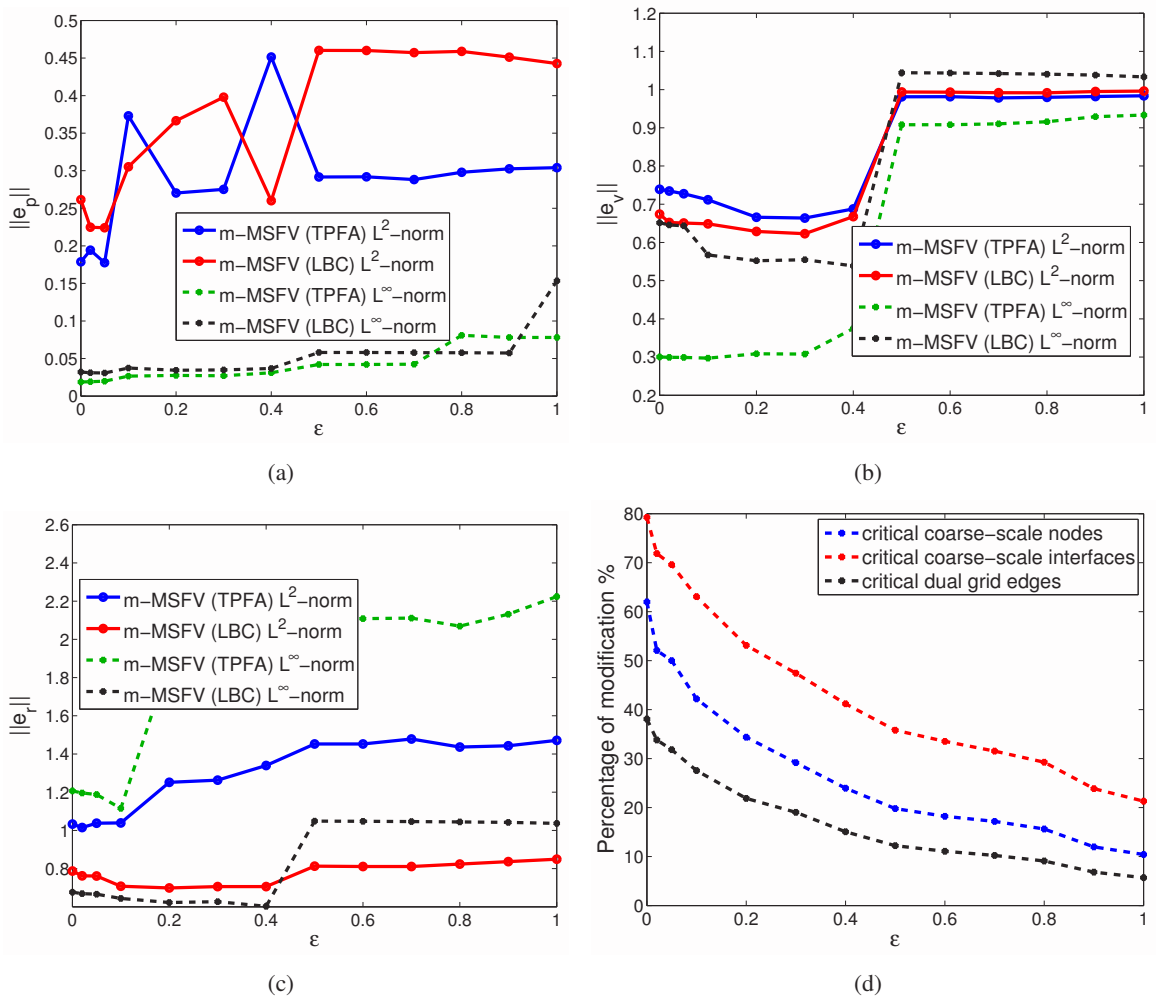

Figure 15 *Error measurements in pressure (a), velocity (b), residual (c) and the computational complexity (d) with different threshold ε for the SPE 10 bottom layer*

Case 2: SPE 10 layers with stretched grid

In this case, both SPE 10 top and bottom layers with stretched grid are examined. The fine-scale and coarse-scale grids are 220×60 and 22×6, respectively. The global boundary conditions are the same as Case 1. The fine-scale grid has an aspect ratio of 10, i.e., $\Delta x = 10\Delta y$. First, for SPE 10 top layer, the permeability field, fine-scale reference, original MSFV and m-MSFV pressure solutions are shown in Figs. 16 and 17. Even though there are no significant peaks in the original MSFV pressure solution, the resulting streamlines of the original MSFV still have circulations. Also, in this case, the m-MSFV (TPFA) approach is using TPFA for almost the entire domain. Therefore, the pressure solution is not accurate. However, m-MSFV(TPFA) can guarantee monotonicity of the pressure distribution, which can be indicated by the circulation-free streamlines (Fig. 19(c)). Circulations can be observed in the streamlines of m-MSFV (LBC) as shown in Fig. 19(d), which implies that m-MSFV (LBC) cannot guarantee a monotone solution in this case. Moreover, the non-monotone solution for original MSFV and m-MSFV (LBC) can be identified by Fig. 18, which indicates that the long-range positive indicators of the coarse-scale system may lead to unphysical multiscale solutions.

Similarly, as shown in Fig. 21, the original MSFV is severely nonmonotone for the SPE 10 bottom layer with stretched grids, and the m-MSFV (LBC) mitigates the issue. However, it cannot fully resolve it. The m-MSFV (TPFA) becomes a global TPFA scheme; therefore, it loses accuracy as indicated in the

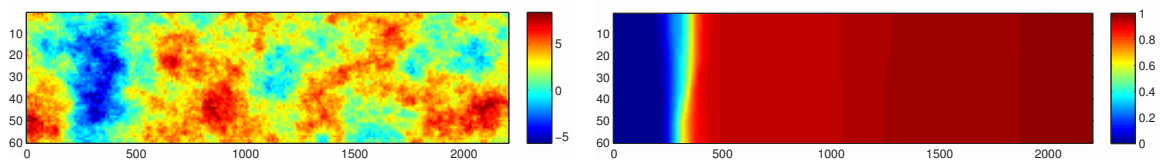

(a) Natural logarithm of the permeability (b) Fine-scale reference pressure

Figure 16 *Permeability and fine-scale pressure solution for the SPE 10 top layer with stretched grids.*

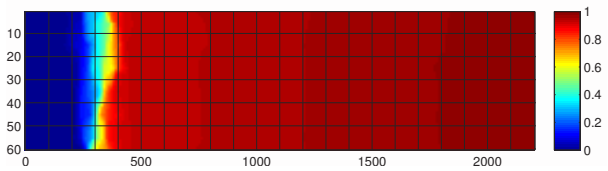

(a) Original MSFV ($\|e_p\|_2 = 0.015$; $\|e_p\|_\infty = 0.148$)

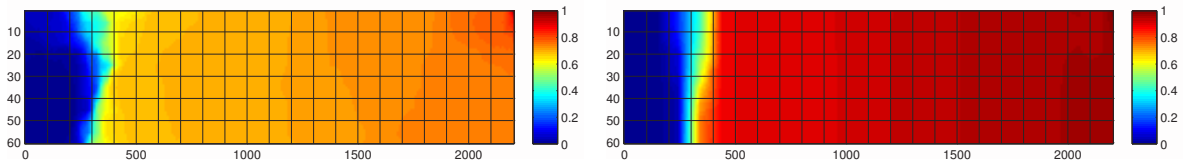

(b) m-MSFV(TPFA) ($\|e_p\|_2 = 0.252$; $\|e_p\|_\infty = 0.407$) (c) m-MSFV(LBC) ($\|e_p\|_2 = 0.034$; $\|e_p\|_\infty = 0.169$)

Figure 17 *Original MSFV and m-MSFV pressure solutions for the SPE 10 top layer with stretched grids, and the relative errors e_p*

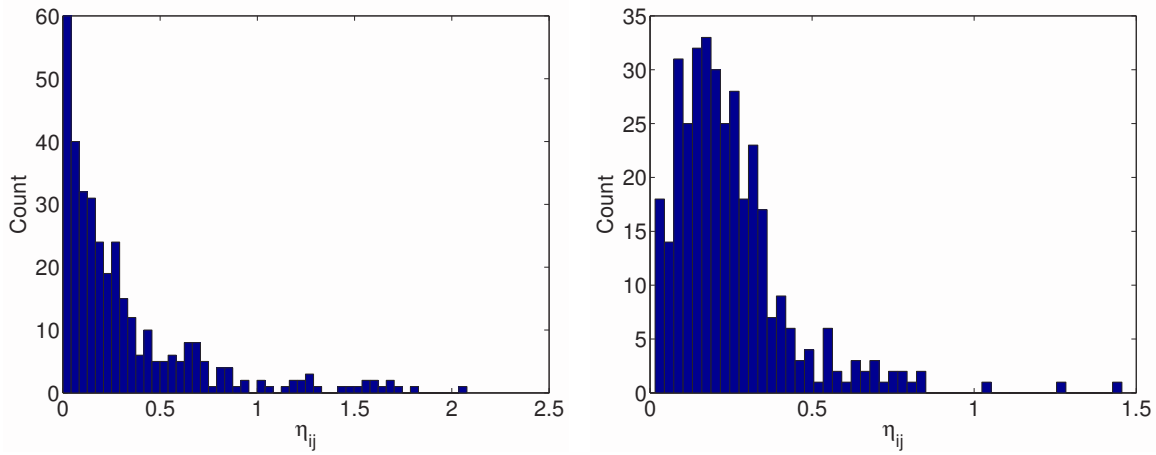

(a) Original coarse-scale system A_c (b) Coarse-scale system A_c with linear BC

Figure 18 *Histogram of η_i of the coarse-scale system A_c for original MSFV (a) and the reconstructed coarse-scale system for m-MSFV (LBC) (b), respectively, for the SPE 10 top layer with stretched grids. Note that m-MSFV (TPFA) eliminates all the positive indicators, therefore the histogram is not shown.*

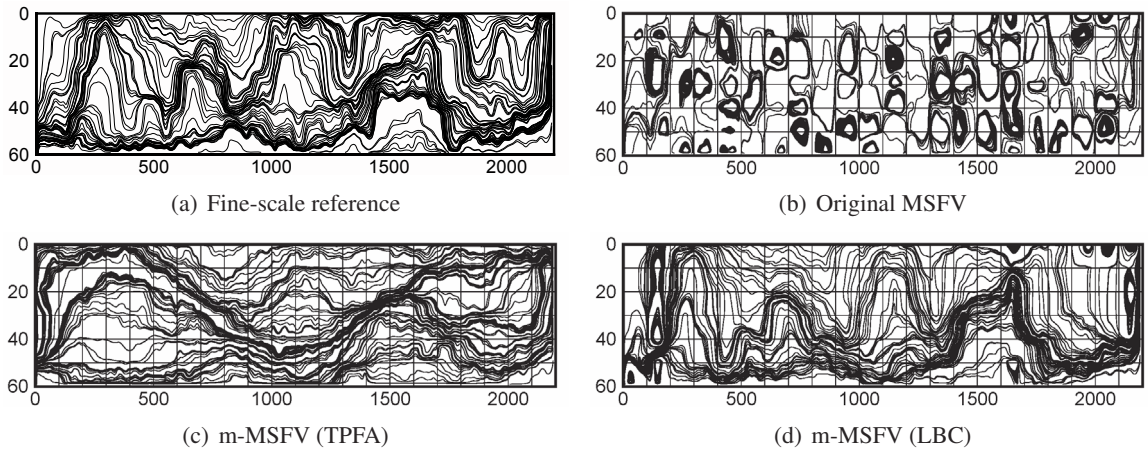

Figure 19 *Streamline plots based on velocity fields reconstructed by fine-scale reference, original and monotone MSFV pressure solutions.*

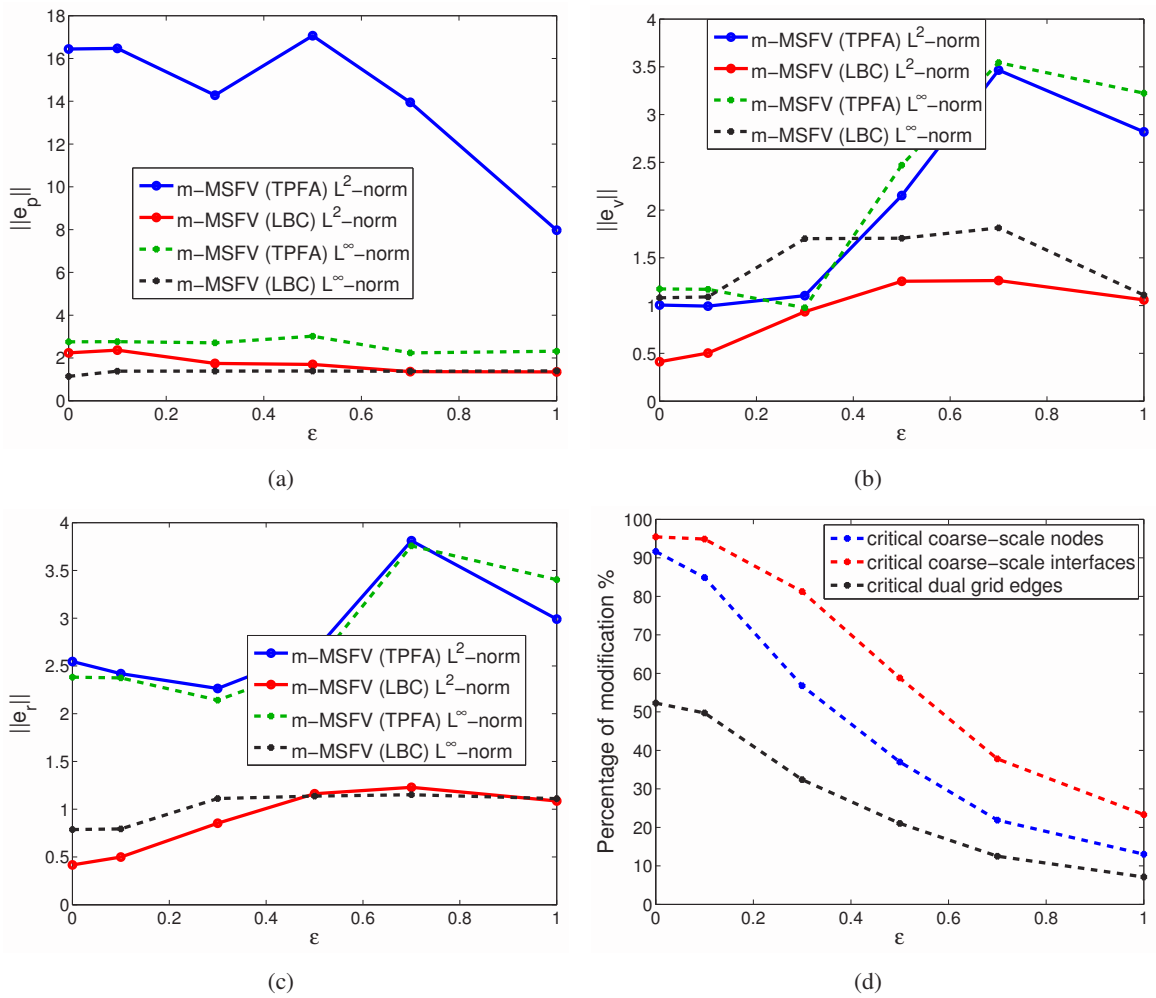

Figure 20 *Error measurements in pressure (a), velocity (b), residual (c) and computational complexity (d) with different threshold ε for the SPE 10 top layer with stretched grids.*

streamline plots shown in Fig. 22. In addition, Figs. 20 and 23 show the accuracy of the m-MSFV method with respect to different strategies and indicate that both m-MSFV(TPFA) and m-MSFV(LBC) have comparable error norms for pressure and velocity.

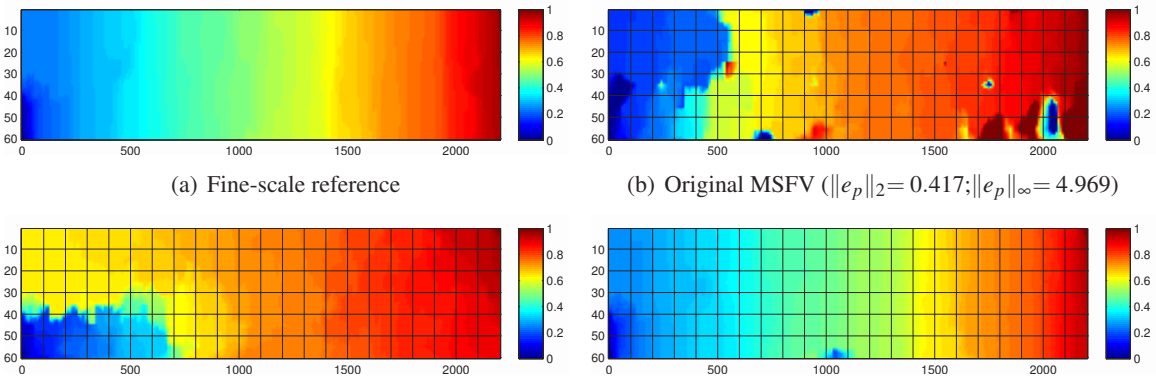

(a) Fine-scale reference

(b) Original MSFV ($\|e_p\|_2 = 0.417; \|e_p\|_\infty = 4.969$)

(c) m-MSFV(TPFA) ($\|e_p\|_2 = 0.338; \|e_p\|_\infty = 0.392$)

(d) m-MSFV(LBC) ($\|e_p\|_2 = 0.043; \|e_p\|_\infty = 0.331$)

Figure 21 *Original MSFV and m-MSFV pressure solutions for the SPE 10 bottom layer with stretched grids, and the relative errors e_p.*

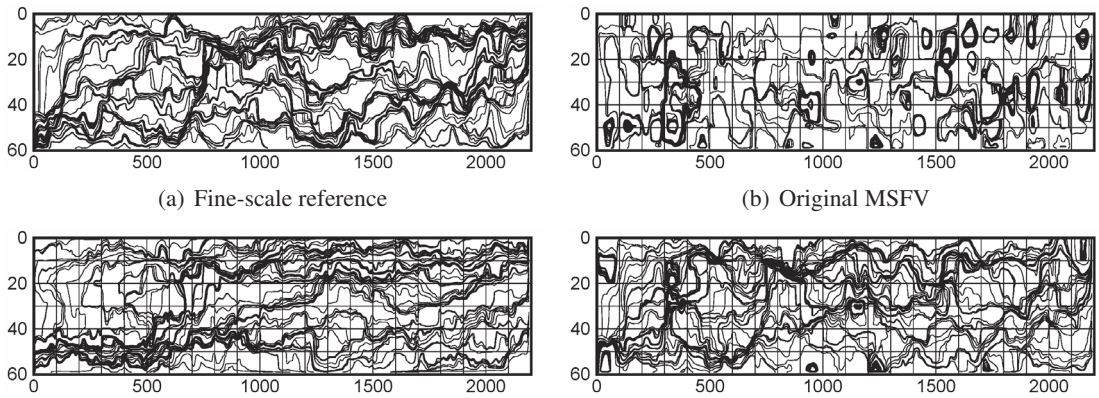

(a) Fine-scale reference

(b) Original MSFV

(c) m-MSFV (TPFA)

(d) m-MSFV (LBC)

Figure 22 *Streamline plots based on velocity fields reconstructed by fine-scale reference, original and m-MSFV pressure solutions for the SPE 10 bottom layer with stretched grids. The coarse-scale grids are indicated by black lines.*

Note that the streamlines given by m-MSFV(LBC) honor the fine-scale reference quite well for the region where no circulations occur. Therefore, it is beneficial to apply m-MSFV(LBC) first, then employ m-MSFV(TPFA) for the places where m-MSFV(LBC) fails to resolve non-physical peaks. Hence, combining both m-MSFV(LBC) and m-MSFV(TPFA) can achieve circulation-free and conservative fine-scale velocity fields without losing accuracy for anisotropic problems. For the SPE 10 top layer with stretched grids, m-MSFV(LBC) is applied first resulting the pressure and velocity distributions as shown in Fig. 17(c) and Fig. 19(d). From Fig. 19(d), m-MSFV(LBC) cannot fully resolve the circulations for some particular regions but results in streamlines that are quite close to fine-scale reference in most regions. In order to remove the circulations, the m-MSFV(TPFA) approach can be employed for the regions where m-MSFV(LBC) is not adequate. With the combination of both approaches, we can obtain the fine-scale pressure and velocity fields shown in Figs. 24 and 25. In additional, the pressure, velocity, and residual errors with respect to the fine-scale reference are given in Table. 1, where we can see that the hybrid m-MSFV delivers the most accurate velocity field.

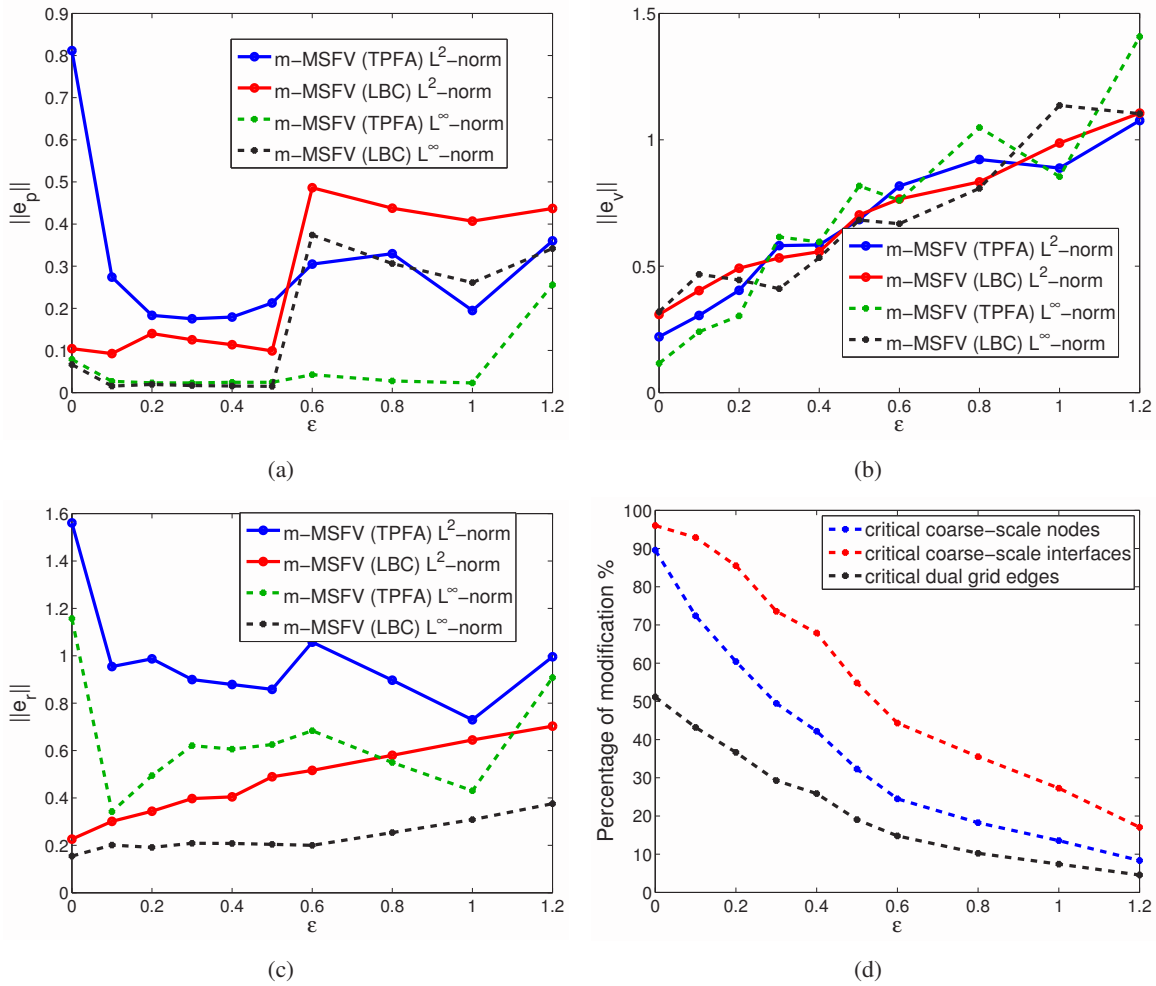

Figure 23 *Error measurements in pressure (a), velocity (b), residual (c) and computational complexity (d) with different threshold ε for SPE 10 bottom layer with stretched grids.*

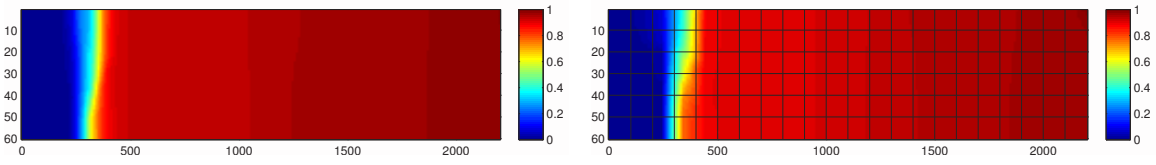

Figure 24 *Pressure distributions for fine-scale reference (a) and obtained by hybrid m-MSFV method (b) for the SPE 10 top layer with stretched grids, i.e.,* $\Delta x = 10\Delta y$.

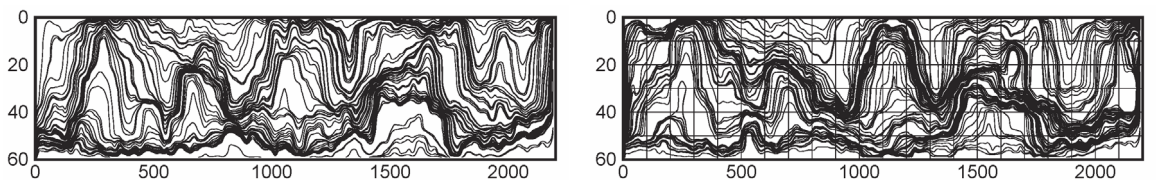

Figure 25 *Velocity distributions for fine-scale reference (a) and obtained by hybrid m-MSFV method (b) for the SPE 10 top layer with stretched grids, i.e.,* $\Delta x = 10\Delta y$.

Error	$\|e_p\|_2$	$\|e_p\|_\infty$	$\|e_v\|_2$	$\|e_v\|_\infty$	$\|e_r\|_2$	$\|e_r\|_\infty$
hybrid m-MSFV	0.034	0.187	0.926	0.585	0.059	0.019
m-MSFV(TPFA)	0.252	0.407	8.165	8.816	0.309	0.052
m-MSFV(LBC)	0.034	0.169	3.349	8.119	0.051	0.017
original MSFV	0.015	0.148	8.115	7.507	0.122	0.022

Table 1 *Relative errors of hybrid m-MSFV, m-MSFV(TPFA), m-MSFV(LBC) and original MSFV for the SPE 10 top layer with stretched grids, i.e.,*$\Delta x = 10\Delta y$.

5. Conclusions

In this paper, a monotone MultiScale Finite Volume (m-MSFV) Method was proposed. The m-MSFV is based on automatic detection of the local interfaces with negative coarse-scale transmissibilities obtained from the integration of fluxes induced by the dual basis functions. Two approaches were developed to fix the non-physical coarse-scale transmissibility, namely, local TPFA and local linear BC approaches. For the first approach, a local TPFA method for the critical interfaces only is used to calculate a positive transmissibility and replace the original MPFA stencils on the coarse-scale system. For the second approach, a linear BC is employed as the local boundary assumption to solve the basis function only for the dual-coarse cells associated with the critical coarse nodes. Then, the coarse-scale system is reconstructed and solved. The local TPFA approach can guarantee monotonicity of the reconstructed fine-scale solution. The local linear BC can mitigate the level of non-monotonicity, but without a guarantee to remove all local pressure oscillations. Therefore, a hybrid strategy that combines both approaches may be effective, whereby the local linear BC approach is used to reduce the degree of non-monotonicity and local TPFA approach is used to achieve the monotonicity for the regions where the linear BC cannot help. Since this m-MSFV method only employs a local fix for critical coarse-cell interfaces that lie in low-permeability regions, the transmissibility values have a small impact on the flow activity. This helps the m-MSFV solution be quite accurate with respect to the fine-scale reference. Moreover, the m-MSFV method is able to optimize the efficiency-monotonicity tradeoff adaptively. Using the m-MSFV method is expected to improve the overall efficiency of sequential fully implicit simulations, which is the focus of our current research.

Acknowledgements

The authors acknowledge financial support from the Petroleum Institute (PI) and the Abu Dhabi National Oil Company (ADNOC).

References

Aziz, K. and Settari, A. [2002] *Petroleum Reservoir Simulation*. Blitzprint Ltd., Cagary, Alberta.

Christie, M.A. and Blunt, M.J. [2001] Tenth SPE comparative solution project: A comparision of upscaling techniques. *SPE Reservoir Evaluation and Engineering*, **4**, 308–317.

Hajibeygi, H., Bonfigli, G., Hesse, M.A. and Jenny, P. [2008] Iterative multiscale finite volume method. *Journal of Computational Physics*, **227**, 8604–8621.

Hajibeygi, H. and Jenny, P. [2009] Multiscale finite-volume method for parabolic problems arising from compressible multiphase flow in porous media. *Journal of Computational Physics*, **228**, 5129–5147.

Hajibeygi, H. and Jenny, P. [2011] Adaptive iterative multiscale finite volume method. *Journal of Computational Physics*, **230**, 628–643.

Hajibeygi, H., Karvounis, D. and Jenny, P. [2011] A hierarchical fracture model for the iterative multiscale finite volume method. *Journal of Computational Physics*, **230**(24), 8729–8743.

Hajibeygi, H., Lee, S.H. and Lunati, I. [2012] Accurate and efficient simulation of multiphase flow in a heterogeneous reservoir by using error estimate and control in the multiscale finite-volume framework. *SPE Journal*, **17**(4), 1071–1083.

Hajibeygi, H. and Tchelepi, H.A. [2014] Compositional multiscale finite-volume formulation. *SPE Journal*, **19**(2), 316–326.

Hesse, M.A., Mallison, B.T. and Tchelepi, H.A. [2008] Compact multiscale finite volume method for heteroge-

neous anisotropic elliptic equations. *SIAM Multiscale Model. Simul.*, **7**, 934–962.
Hou, T. and Wu, X.H. [1997] A multiscale finite element method for elliptic problems in composite matrials and porous meida. *Journal of Computational Physics*, **134**, 169–189.
Jenny, P., Lee, S.H. and Tchelepi, H.A. [2003] Multi-scale finite-volume method for elliptic problems in subsurface flow simulation. *Journal of Computational Physics*, **187**, 47–67.
Jenny, P., Lee, S.H. and Tchelepi, H.A. [2006] Adaptive fully implicit multi-scale finite-volume method for multiphase flow and transport in heterogeneous porous media. *Journal of Computational Physics*, **217**, 627–641.
Jenny, P. and Lunati, I. [2009] Modeling complex wells with the multi-scale finite volume method. *Journal of Computational Physics*, **228**, 687–702.
Lee, S.H., Wolfsteiner, C. and Tchelepi, H.A. [2008] Multiscale finite-volume formulation for multiphase flow in porous media: black oil formulation of compressible, three-phase flow with gravity. *Comput. Geosci.*, **12**(3), 351–366.
Lee, S.H., Zhou, H. and Tchelepi, H.A. [2009] Adaptive multiscale finite-volume method for nonlinear multiphase transport in heterogeneous formations. *Journal of Computational Physics*, **228**(24), 9036–9058.
Lunati, I. and Jenny, P. [2007] Treating highly anisotropic subsurface flow with the multiscale finite-volume method. *SIAM Multiscale Model. Simul.*, **6**(1), 308–318.
Wang, Y., Hajibeygi, H. and Tchelepi, H.A. [2014] Algebraic multiscale solver for flow in heterogeneous porous media. *Journal of Computational Physics*, **259**, 284–303.
Wolfsteiner, C., Lee, S.H. and Tchelepi, H.A. [2006] Well modeling in the multiscale finite volume method for subsurface flow simulation. *SIAM Multiscale Model. Simul.*, **5**(3), 900–917.
Zhou, H., Lee, S.H. and Tchelepi, H.A. [2011] Multiscale finite-volume formulation for saturation equations. *SPE Journal*, **17**(1), 198–211.
Zhou, H. and Tchelepi, H.A. [2008] Operator-based multiscale method for compressible flow. *SPE Journal*, **13**, 267–273.
Zhou, H. and Tchelepi, H.A. [2012] Two-stage algebraic multiscale linear solver for highly heterogeneous reservoir models. *SPE Journal*, **17**(2), 523–539.